Chinese Chemical Letters 35 (2024) 109114

Contents lists available at ScienceDirect

Chinese Chemical Letters

journal homepage: www.elsevier.com/locate/cclet

The Mn/Yb/Er triple-doped CeO_2 nanozyme with enhanced oxidase-like activity for highly sensitive ratiometric detection of nitrite

Simin Wei[a], Yaqing Yang[a], Junjie Li[a], Jialin Wang[a], Jinlu Tang[b], Ningning Wang[a,*], Zhaohui Li[a,*]

[a] College of Chemistry, Institute of Analytical Chemistry for Life Science, Henan Joint International Research Laboratory of Green Construction of Functional Molecules and their Bioanalytical Applications, Zhengzhou University, Zhengzhou 450001, China
[b] School of Basic Medical Sciences, Zhengzhou University, Zhengzhou 450001, China

ARTICLE INFO

Article history:
Received 13 April 2023
Revised 31 August 2023
Accepted 15 September 2023
Available online 18 September 2023

Keywords:
$Mn/Yb/Er/CeO_2$ nanozyme
Oxidase-like activity
Nitrite
Ratiometric detection
Two-detection mode

ABSTRACT

Long-term excessive intake of nitrite (NO_2^-) poses a great threat to human health, needing a simple and fast method to detect NO_2^- in food. Herein, *via* a simple and feasible strategy, Mn/Yb/Er triple-doped CeO_2 nanozyme ($Mn/Yb/Er/CeO_2$) was synthesized for highly sensitive ratiometric detection of nitrite. By doping Mn, Yb, Er into CeO_2 lattice structure, $Mn/Yb/Er/CeO_2$ nanozyme showed enhanced oxidase-like activity, obtaining a higher density of oxygen vacancy and a higher ratio of Ce^{3+} to Ce^{4+} than that of CeO_2. The 3,3′,5,5′-tetramethylbenzidine (TMB) can be effectively oxidized by $Mn/Yb/Er/CeO_2$ to produce the oxidized TMB (oxTMB), showing a significant absorption signal at 652 nm. Additionally, nitrite can react with oxTMB to produce yellow diazotized oxTMB, which is accompanied by an elevated absorption signal at 445 nm and a decreased absorption signal at 652 nm. Thus, based on the oxidase-mimetic activity of $Mn/Yb/Er/CeO_2$ and the diazotization reaction between NO_2^- and oxTMB, a ratiometric colorimetric assay was established for NO_2^- detection in food. Furthermore, by integrating $Mn/Yb/Er/CeO_2$ with a smartphone, a colorimetric smartphone-sensing platform was successfully fabricated for visualization and quantitative detection of NO_2^-. Notably, this two-detection mode showed excellent sensitivity, selectivity, reliability and practicability in monitoring the NO_2^- in real samples, impling its great potential for food safety.

Nitrite (NO_2^-), a food additive, is widely found in drinking water and food [1]. However, *N*-nitrosamine molecules, which are extremely carcinogenic, can be produced after amines, amides or proteins interact with nitrite. Human health is seriously threatened by long-term excessive nitrite consumption [2,3]. Thus, it is desired to develop a simple and fast method for nitrite detection in food. Currently, different methods including electrochemistry [4], fluorometry [5–7], gas chromatography [8] have been developed to detect NO_2^-. However, these conventional methods usually face some shortcomings, including requirements of bulky and expensive equipment or expert skills, complex operation and time-consuming procedures. Compared with the abovementioned methods, colorimetric assay based on the measurement of colored compounds has attracted increasing attention by taking advantage of its low cost, easy operation, rapid visual detection and potential for on-site application. However, constructing a catalyst with excellent efficiency is a key step to effectively improve colorimetric changes and achieve excellent detection performance in colorimetric assay.

Nanozyme is a kind of nanomaterial with intrinsic enzymatic activities, possessing splendid advantages such as good stability, high catalytic activity, low cost, desired reusability and fine adaptability to environment [9,10]. With these features, nanozyme has been extensively used in the aspect of biochemical sensing, biomedicine, food industry and environmental science [11–13]. Notably, nanozymes have been widely utilized to catalyze the chromogenic substrates in various colorimetric sensing applications, and provide catalytic amplification signals for highly sensitive detection [14–16]. Currently, nanoceria (CeO_2) has been confirmed to have a wide variety of enzymatic activities, such as oxidase (OXD), peroxidase (POD), phosphatase, nuclease, and urease owing to the abundance of oxygen vacancies and the conversion between the Ce(III)/Ce(IV) valence states [17–21]. Thus, CeO_2 as a fascinating sensor material has been extensively used to detection various analytes [17,22]. Generally, the catalytic performance of CeO_2 is the core of the colorimetric probe. Thus, the rational design of CeO_2

* Corresponding authors.
E-mail addresses: ningningwang@zzu.edu.cn (N. Wang), zhaohui.li@zzu.edu.cn (Z. Li).

https://doi.org/10.1016/j.cclet.2023.109114
1001-8417/

with high catalytic performance is significant to meet the demand of detection sensitivity in practical application. Recently, the strategy of doping metal ions has played an irreplaceable role in regulating the catalytic activity of nanoceria [23,24]. Numerous studies have shown that doping pure CeO_2 with other metal ions can realize the enhancement of multi-enzyme-like activities through increasing the concentration and migration of oxygen vacancies [25–28]. Mn has obtained great attention due to its changeable oxidation state and better redox behavior. The doping of Mn^{2+} can cause the reconstruction of CeO_2 structure, accelerate the production of oxygen vacancies and the conversion of Ce^{4+} to Ce^{3+} [26]. Furthermore, lanthanide ions with ionic radius and electronegativity close to those of cerium are thought to be the most appropriate modifiers of ceria, which facilitates its easy incorporation into the crystal lattice of CeO_2. Usually, when Ce^{4+} ions are substituted with lanthanide ions, introducing stress into ceria lattice to execute charge neutrality and nonstoichiometry compensation, enhances oxygen storage capacity from lattice to its surface and decreases the activation energy for the formation of oxygen vacancy [29]. A novel Er and Yb codoped CeO_{2-x} showed higher enzyme-like catalytic activity than that of CeO_{2-x}, because the doping of Yb and Er ions can generate extra oxygen vacancies [30]. Co-doping is an effective method for increasing the catalytic performance of CeO_2. Metal ions such as Mn^{2+}, Yb^{3+} and Er^{3+} can be chosen as possible co-dopants to improve the structural, surface, and redox properties of CeO_2. A synergistic effect can be expected, such as the redox cycles Ce^{3+}/Ce^{4+} and $Mn^{4+}/Mn^{3+}/Mn^{2+}$ ions, the increased conversion process of Ce^{4+} to Ce^{3+}, and the enhanced number of defective sites (*e.g.*, oxygen vacancies), which is required for the catalytic activity. Additionally, previous metal doping CeO_2 nanozymes are usually prepared by rigorous methods and complex synthetic processes, such as high temperature and high pressure, which restricts their practical applications. Therefore, constructing a high-performance codoped CeO_2 nanozyme *via* a facile and efficient strategy is highly desirable to extent their practical applications.

Herein, *via* a simple and feasible strategy, Mn/Yb/Er triple-doped CeO_2 nanozyme ($Mn/Yb/Er/CeO_2$) was synthesized for highly sensitive ratiometric detection of nitrite. By doping Mn, Yb, Er into CeO_2 lattice structure, $Mn/Yb/Er/CeO_2$ showed enhanced oxidase-like activity, obtaining a higher density of oxygen vacancy and a higher ratio of Ce^{3+} to Ce^{4+} than that of CeO_2. The 3,3′,5,5′-tetramethylbenzidine (TMB) can be effectively oxidized by $Mn/Yb/Er/CeO_2$ to produce the oxidized TMB (oxTMB), showing a significant absorption signal at 652 nm. Additionally, nitrite can react with oxTMB to produce yellow diazotized oxTMB, which is accompanied by an elevated absorption signal at 445 nm and a decreased absorption signal at 652 nm. Thus, based on the oxidase-mimetic activity of $Mn/Yb/Er/CeO_2$ and the diazotization reaction between NO_2^- and oxTMB, a ratiometric colorimetric assay was established for NO_2^- detection in food (Scheme 1). Furthermore, by integrating $Mn/Yb/Er/CeO_2$ with a smartphone, a colorimetric platform was successfully fabricated for visualization and quantitative detection of NO_2^-. Notably, this two-detection mode (colorimetric spectrophotometer mode and smartphone-sensing platform) showed excellent sensitivity, selectivity, reliability and practicability in monitoring the NO_2^- in real samples, implying its great potential for food safety.

To improve the oxidase mimicking activity of CeO_2, Mn/Yb/Er were utilized to doping into the lattice structure of CeO_2. First, *via* low-temperature hydrothermal method, CeO_2 and doped CeO_2 nanozymes (Mn/CeO_2 and $Mn/Yb/Er/CeO_2$) were prepared. Then, the as-prepared nanozymes were modified with citrate to improve their water-solubility and stability. As illustrated in Fig. S1 (Supporting information), zeta-potential of the citrate modified $Mn/Yb/Er/CeO_2$ was −40 mV, and significantly negative-shifted

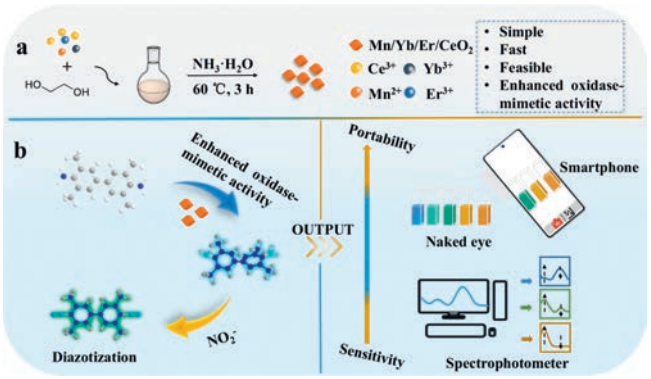

Scheme 1. Schematic illustration of nitrite detection based on a novel triple metal ion doped CeO_2 nanozyme ($Mn/Yb/Er/CeO_2$). (a) Strategy for fabrication of Mn/Yb/Er/ CeO_2 nanozyme. (b) Working principle for ratiometric assay of nitrite.

compared with that of the bared $Mn/Yb/Er/CeO_2$ (15 mV). Similarly, other nanozymes with the modifying of citrate also showed electronegative.

Next, the crystal structures of CeO_2, Mn/CeO_2, and $Mn/Yb/Er/CeO_2$ were identified by X-ray diffraction (XRD). The characteristic peaks at 28.8°, 33.3°, 47.7°, 56.5°, 69.6°, and 76.7° shown in Fig. S2 (Supporting information) can be ascribed respectively to the diffraction planes of (111), (200), (220), (311), (400), and (331) of cubic fluorite structured of CeO_2 (PDF# 43–1002), indicative of the CeO_2 structure of the prepared nanozymes. Notably, owing to the incorporation of smaller atomic radius ions (Mn, Yb, and Er) (Table S1 in Supporting information) into CeO_2, a shift and broadening of the diffraction peak ascribed to (111) were observed in the sample of Mn/CeO_2 and $Mn/Yb/Er/CeO_2$. This phenomenon was consistent with the results reported in the literatures [24,31]. Furthermore, the transmission electron microscopy (TEM) and high-resolution TEM (HRTEM) images of CeO_2, Mn/CeO_2, and $Mn/Yb/Er/CeO_2$ were conducted. Fig. 1a revealed that the lattice spacing of the (111) plane of CeO_2 (0.328 nm) was larger than that of doped CeO_2 (Mn/CeO_2: 0.320 nm, and $Mn/Yb/Er/CeO_2$: 0.310 nm), which was consistent with XRD data. This may be explained by the incorporation of smaller atomic radius ions (Mn, Yb, and Er) into the lattice structure of CeO_2. Additionally, elemental mapping analysis of $Mn/Yb/Er/CeO_2$ indicated that Ce, Mn, Yb, Er, and O were evenly distributed in the sample (Fig. 1b).

To distinguish crystallization or defects of samples and provide more information on the surface of samples, Raman spectra were obtained and illustrated in Fig. S3 (Supporting information). A sharp Raman peak around 460 cm^{-1} related to the F_{2g} characteristic vibration peak of CeO_2 were observed in all three samples, which was attributed to the symmetrical stretching vibration of oxygen atoms around cerium ion (Ce-8O) in ceria lattice. Additionally, F_{2g} peaks of doped CeO_2 was shifted and widened

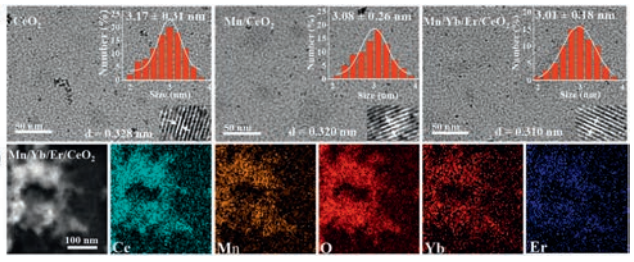

Fig. 1. (a) TEM images with size distribution and HRTEM images (insets) of CeO_2, Mn/CeO_2, and $Mn/Yb/Er/CeO_2$. (b) EDS-mapping images of $Mn/Yb/Er/CeO_2$.

compared with that of CeO_2, indicating that O atoms around Ce ion have been altered. In general, an obvious Raman band around 600–615 cm^{-1} usually indicated the formation of oxygen vacancies. The oxygen vacancy Raman peak of CeO_2 was found at 603 cm^{-1}, while that of Mn/Yb/Er/CeO_2 and Mn/CeO_2 was 615 cm^{-1}. The peak area ratio of the oxygen vacancy Raman peak (615 cm^{-1} or 603 cm^{-1}) to the F_{2g} characteristic vibration peak (460 cm^{-1}), defined as A_{615}/A_{460} or A_{603}/A_{615}, is used to represent the oxygen vacancy relative concentration. It can be found from Fig. S3 that the ratio gradually increases with metal ion doping (Mn/Yb/Er/CeO_2 > Mn/CeO_2 > CeO_2). This result suggested that Mn/Yb/Er/CeO_2 has the highest concentration of oxygen vacancies.

To further elucidate the chemical composition and valence state of material in detail, the X-ray photoelectron spectroscopy (XPS) tests were conducted. The full XPS of Mn/Yb/Er/CeO_2 showed that Ce, Mn, Yb, Er, and O were found present in the sample (Fig. S4 in Supporting information). Fig. S5a (Supporting information) depicts the Ce XPS spectra of three samples. The binding energies at 900.7, 906.7, 916.2, 883.0, 887.6, and 897.8 eV can be ascribed to surface Ce^{4+}, while binding energies at 903.3, 899.5, 881.5 and 885.2 eV are assigned to Ce^{3+}. Compared to CeO_2 and Mn/CeO_2, Mn/Yb/Er/CeO_2 has the highest Ce^{3+}/Ce^{4+} concentration ratio on the surface, indicating that the introduction of Mn/Yb/Er can increase the amount of Ce^{3+} species and improve the catalytic activities of Mn/Yb/Er/CeO_2. Oxygen vacancy is a typical anionic defect that plays a very important role in surface catalytic reactions [32]. Then, the peak deconvolutions of the O 1s XPS spectra of three samples were investigated (Fig. S5b in Supporting information). The surface oxygen species (529.9–531.5 eV; O_α) and lattice oxygen (528.5–529.5 eV; O_β) are all present in the O 1s XPS spectrum. The surface oxygen vacancy change can be represented by using the percentage of O_α [31]. Mn/Yb/Er/CeO_2 possesses the higher ratio of O_α/O_β (1.74) than that of CeO_2 (1.36) and Mn/CeO_2 (1.04), indicating that the surface of Mn/Yb/Er/CeO_2 has higher density of oxygen vacancies. The O 1s XPS spectra results were consistent with the Raman data.

As a chromogenic substrate, TMB was employed to conduct a typical chromogenic reaction. Then, the oxidase-like activity of Mn/Yb/Er/CeO_2 was evaluated. Fig. 2a showed that neither UV–vis absorbance nor apparent color changes were observed in the solution with only Mn/Yb/Er/CeO_2 or TMB. When Mn/Yb/Er/CeO_2 was added into TMB solution with dissolved O_2, apparent color changes from colorless to blue were observed, and a maximum absorbance at 652 nm appeared, owing to the production of oxTMB. This result implied that Mn/Yb/Er/CeO_2 is important in the redox reaction between TMB and O_2. Notably, the production of oxTMB was partially inhibited in N_2-saturated buffer, accompanied by an obvious reduce of the absorbance intensity at 652 nm. The result confirmed that the TMB oxidation reaction is dependent on dissolved O_2, and Mn/Yb/Er/CeO_2 acts as an oxidase-like nanozyme in the catalytic oxidation of TMB. In general, reactive oxygen species (ROS) produced by dissolved O_2 plays an important role in the oxidative reaction. Thus, the influence of ROS on this reaction was investigated to confirm the catalytic mechanism of Mn/Yb/Er/CeO_2. ROS like $O_2^{\bullet-}$, $^{\bullet}OH$, $^1O_2$ can be captured by *p*-benzoquinone (PBQ), isopropanol alcohol (IPA), and tryptophan (Trp), respectively. As depicted in Fig. 2b, the presence of PBQ reduced the production of oxTMB, reducing its absorbance intensity at 652 nm, while IPA and Trp had less effect on this process. This phenomenon suggested that $O_2^{\bullet-}$ radicals were generated during oxidative reaction. Based on above mentioned analysis, it is reasonable to infer that Mn/Yb/Er/CeO_2 may first catalyzes O_2 to generate $O_2^{\bullet-}$ radicals, thus oxidizing TMB to oxTMB.

Generally, reaction duration, nanozyme concentration, buffer pH, and temperature have a significant impact on the catalytic activity of nanozymes. To maximally present the oxidase-like activity of Mn/Yb/Er/CeO_2 in TMB solution with dissolved O_2, reaction conditions as above mentioned were optimized. As depicted in Fig. S6a (Supporting information), a plateau and steady state of the absorbance intensity at 652 nm was reached after 10 min. Thus, 10 min was utilized as the TMB oxidation time in the following study. Fig. S6b (Supporting information) demonstrated the absorbance intensity of oxTMB increases with the increasing amounts of Mn/Yb/Er/CeO_2. To ensure the assay results more accurate, 25 μg/mL was chosen as the amount of Mn/Yb/Er/CeO_2 in the following study. As shown in Fig. S6c (Supporting information), the catalytic activity of Mn/Yb/Er/CeO_2 changed with altered buffer pH, with maximum activity at pH 3.0. When the temperature ranged from 25 °C to 65 °C, Mn/Yb/Er/CeO_2 consistently showed excellent catalytic activity (Fig. S6d in Supporting information). Given the convenience of operation, 25 °C was selected.

To further evaluate the oxidase-mimicking ability of Mn/Yb/Er/CeO_2, we conducted the steady-state kinetic analysis under optimal conditions. Correlation of initial reaction velocity with different concentrations of TMB was shown in Fig. 2c. According to the Lineweaver-Burk double reciprocal graph, the maximum velocity (V_{max}) and the apparent Michaelis-Menten constant (K_m) were calculated to 0.2068 μmol L^{-1} s^{-1} and 45.54 μmol/L (Fig. 2d). Meanwhile, CeO_2 and Mn/CeO_2 was also investigated under optimal conditions (Fig. S7 in Supporting information). As compared in Fig. S8 (Supporting information), the apparent K_m value obtained by Mn/Yb/Er/CeO_2 was lower than that of CeO_2 and Mn/CeO_2, indicating that Mn/Yb/Er/CeO_2 has a stronger affinity toward TMB. Moreover, Fig. S9 (Supporting information) revealed that Mn/Yb/Er/CeO_2 exhibits a higher activity in catalyzing the TMB oxidation reaction than that of CeO_2 and Mn/CeO_2. This may be attributed to Mn/Yb/Er/CeO_2 has higher density of oxygen vacancies and Ce^{3+}/Ce^{4+} content ratio. In addition, Mn/Yb/Er/CeO_2 showed excellent oxidase-like catalytic stability even after a prolonged storage, which facilitates its application in the field of analysis (Fig. S10 in Supporting information).

Interestingly, the UV-vis absorption spectra of the Mn/Yb/Er/CeO_2 + TMB solution was significantly altered when the nitrite was added. As exhibited in Fig. S11a (Supporting information), a new UV-vis absorption peak appeared at 445 nm when nitrite was present, while the peak at 652 nm was reduced. Addi-

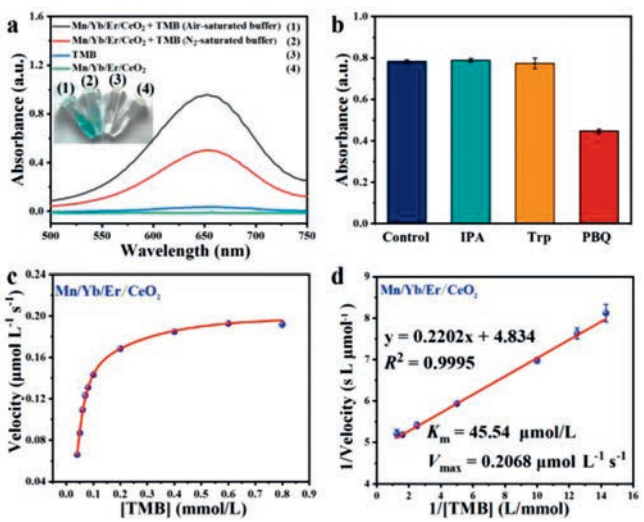

Fig. 2. (a) Absorption spectrum and the corresponding photograph of Mn/Yb/Er/CeO_2 + TMB (air-saturated buffer), Mn/Yb/Er/CeO_2 + TMB (N_2-saturated buffer), TMB, and Mn/Yb/Er/CeO_2. (b) The effect of different scavenger on [Mn/Yb/Er/CeO_2 + TMB] system. (c) The relation curve of velocity with different TMB concentrations. (d) Lineweaver-Burk diagram of Mn/Yb/Er/CeO_2.

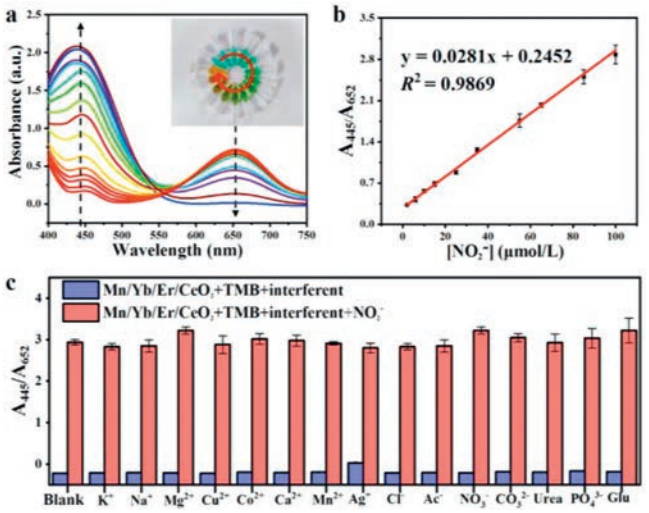

Fig. 3. (a) UV–vis spectra of [Mn/Yb/Er/CeO_2 + TMB] system with the concentration of NO_2^-. (b) The linear calibration plot of NO_2^- sensing. (c) Selectivity and anti-interference ability experiment of [Mn/Yb/Er/CeO_2 + TMB] system for NO_2^-.

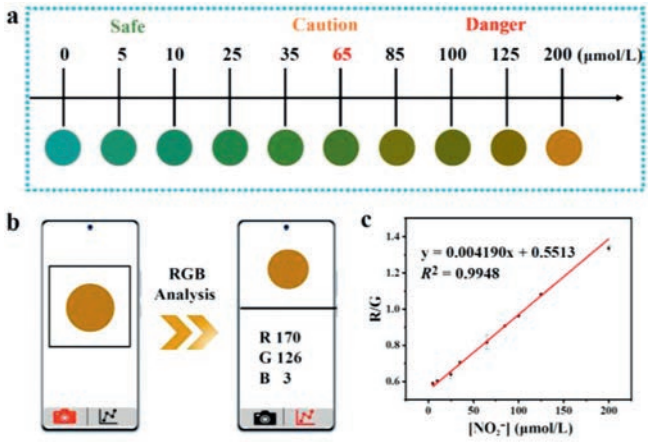

Fig. 4. (a) Colorimetric pictures of samples with different content of NO_2^-. (b) RGB analysis of the various color pictures using a color recognition APP. (c) The corresponding linear relationship of R/G values of samples pictures *vs.* NO_2^- concentrations.

tionally, the solution's color was changed from blue to green (inset in Fig. S11a). This phenomenon may be ascribed to the occurrence of the diazidation reaction between the nitrite and oxTMB intermediate under the acidic condition. As illustrated in Fig. S11b (Supporting information), a diazonium salt (diazotizated oxTMB) can be formed by the reaction between nitrite with the aromatic primary amine group of the oxTMB under the acidic condition (pH 3.0). Next, an ascorbic acid (AA) reduction test was conducted to verify this conclusion. As demonstrated in Fig. S12 (Supporting information), AA can reduce oxTMB, overoxidized oxTMB, and the mixture of oxTMB and overoxidized oxTMB to colorless TMB [33]. However, when NO_2^- was present in Mn/Yb/Er/CeO_2 + TMB solution, the diazotized oxTMB was produced by the diazotization reaction. Notably, AA cannot reduce the produced diazotized oxTMB to colorless TMB. This phenomenon demonstrated the occurrence of diazozation reaction.

Based on the above mechanisms, Mn/Yb/Er/CeO_2 + TMB solution system was developed for nitrite detection. Diazozation reaction time was optimized firstly to better detect nitrite. Fig. S13 (Supporting information) displayed that the ratio of the absorbance intensity of reaction solution at 445 nm to that at 652 nm (A_{445}/A_{652}) obtained a plateau and steady state after 30 min. Thus, 30 min was utilized as diazozation reaction time in the following study. The detection sensitivity of Mn/Yb/Er/CeO_2 + TMB solution system to nitrite was investigated. With gradually increased concentration of nitrite, the absorbance intensity increased significantly at 445 nm. Simultaneously, the absorbance intensity decreased at 652 nm during the experiments (Fig. 3a). Accordingly, the color of solution was also changed obviously as shown in the inset in Fig. 3a, which demonstrated the detection feasibility of nitrite. In Fig. 3b, the absorption ratio A_{445}/A_{652} increased gradually with the increase of NO_2^- concentration. A_{445}/A_{652} displayed a good linearity for nitrite at 2.0–100 μmol/L ($R^2 = 0.9869$), and the limit of detection (LOD) was 0.29 μmol/L. Additionally, TMB can directly react with nitrite under acidic solution to produce diazonium salts with an obvious absorption signal at 445 nm [34]. Thus, single-signal colorimetric detection mode based on TMB + NO_2^- solution system was investigated. A_{445} displayed a good linearity for nitrite at 35–150 μmol/L ($R^2 = 0.9963$), and the LOD was 1.3 μmol/L (Fig. S14 in Supporting information). In contrast, the sensitivity and LOD of the ratiometric colorimetric detection mode is superior to that of the single-signal colorimetric detection mode. Next, the selectivity and anti-interference ability of this ratiometric colorimetric assay were investigated by detecting nitrite (100 μmol/L) with or without other interferences species (1 mmol/L). Interferences such as K^+, Na^+, Ca^{2+}, Mn^{2+}, Mg^{2+}, Ag^+, Cl^-, Ac^-, NO_3^-, CO_3^{2-}, PO_4^{3-}, urea, and glucose interfere very little on the nitrite analysis, illustrating this method has excellent selectivity and anti-interference ability for nitrite detection (Fig. 3c). These excellent performances of this method may result from the cascade of oxidase-like catalysis and diazidation.

Recently, smartphone-based portable sensing platforms have been widely developed due to their advantages of accessibility and portability [35,36]. Additionally, the accuracy and resolution of smartphone-sensing platforms exceed visual detection. Thus, by integrating Mn/Yb/Er/CeO_2 with a smartphone, a colorimetric smartphone-sensing platform was fabricated for visualization and quantitative detection of NO_2^-. Smartphone was employed as the signal readout to enable portable nitrite detection. The photos of samples with nitrite concentration from 0 to 200 μmol/L were taken by a smartphone, showing the color transition from blue to yellow (Fig. 4a). Then, these photos were analyzed by the color recognition APP, and further converted into RGB (red, green and blue) values to achieve portable nitrite detection (Fig. 4b). The ratio of R and G (R/G) showed a good linearity for nitrite at 5–200 μmol/L (R/G = 0.004190 [NO_2^-] + 0.5513, $R^2 = 0.9948$) with a LOD of 3.3 μmol/L (Fig. 4c). Compared with the ratiometric colorimetric assay on the absorption spectrometer, the smartphone-sensing platform has the merits of low cost, flexibility, portability, and wider detection ranges. Furthermore, the performance of our assays (colorimetric spectrophotometer mode and smartphone-sensing platform) are comparable or better than those of reported methods for nitrite detection (Table S2 in Supporting information). The above results revealed that this smartphone-sensing platform has the potential application for the on-site of nitrite detection.

To evaluate the reliability, feasibility and practicality of our method, real samples including Tap water, Mei Lake water, pickle water and sausage were selected to detect nitrite. Samples were pretreated according to previous literature reports [3]. As shown in Table S3 (Supporting information), the spiked recoveries ranged from 95.3% to 101.0% for the colorimetric spectrophotometer mode, and 94.3% to 108.1% for the smartphone-sensing platform, implying the wonderful feasibility and practicality of the two-detection mode for nitrite detection in real samples. Furthermore, to check the accuracy of our method, all samples were simultaneously de-

termined by a commercial detection kit. The results showed that the nitrite concentration detected by colorimetric spectrophotometer mode and smartphone-sensing platform were almost consistent with that measured by the commercial detection kit, indicating that our two-detection mode has the reliable and potential applications in food safety.

In this work, Mn/Yb/Er/CeO_2 with enhanced oxidase-like activity was successfully prepared by a low-temperature hydrothermal method. The oxygen vacancies and Ce^{3+} concentration of Mn/Yb/Er/CeO_2 were efficiently improved by doping Mn/Yb/Er. Take advantage of the excellent oxidase-mimetic activity of Mn/Yb/Er/CeO_2 and the diazotization reaction between NO_2^- and oxTMB, a ratiometric colorimetric assay was established for NO_2^- detection in food. Beside the fabrication of colorimetric spectrophotometer mode, a smartphone-sensing platform based on this detection system and smartphone was successfully fabricated for visualization and quantitative detection of NO_2^-. Notably, this two-detection mode showed excellent reliability and practicability in monitoring the NO_2^- in real samples. This work not only provides a method for preparing nanozymes with enhanced oxidase mimic activity, but also implies its great potential for food safety.

Declaration of competing interest

The authors declare that they have no known competing financial interests or personal relationships that could have appeared to influence the work reported in this paper.

Acknowledgments

The work was supported by the National Natural Science Foundation of China (Nos. 22004111 and 21974125), the Tackle Key Problems in Science and Technology Project of Henan Province, China (No. 222102310386), China Postdoctoral Science Foundation (No. 2020M682327), Henan Postdoctoral Foundation (No. 202002009), Program for Innovative Research Team (in Science and Technology) in University of Henan Province (No. 22TRTSTHN002), and Excellent Youth Foundation of Henan Scientific Committee (No. 232300421021).

Supplementary materials

Supplementary material associated with this article can be found, in the online version, at doi:10.1016/j.cclet.2023.109114.

References

[1] W. Li, X. Wen, H. Zhao, et al., ACS Appl. Nano Mater. 3 (2020) 11838–11849.
[2] Y. Hao, Z. Yang, W. Dong, et al., J. Hazard. Mater. 430 (2022) 128393.
[3] M. Wang, P. Liu, H. Zhu, B. Liu, X. Niu, Biosensors 11 (2021) 280.
[4] S. Dong, M. Tong, D. Zhang, et al., Sens. Actuator. B 251 (2017) 650–657.
[5] J. Jia, W. Lu, L. Li, et al., J. Mater. Chem. B 8 (2020) 2123–2127.
[6] H. Tao, Z. Zhang, Q. Cao, et al., RSC Adv. 12 (2022) 12655–12662.
[7] J.X. Wu, B. Yan, Ind. Eng. Chem. Res. 57 (2018) 7105–7111.
[8] M.G. Seid, K. Cho, C. Lee, et al., Sci. Total Environ. 633 (2018) 352–359.
[9] H. Ding, B. Hu, B. Zhang, et al., Nano Res. 14 (2021) 570–583.
[10] D. Li, D. Dai, G. Xiong, et al., Small 19 (2023) 2205870.
[11] X. Liu, J. Yang, J. Cheng, et al., Sens. Actuators B 337 (2021) 129763.
[12] Z. Lu, Y. Dang, C. Dai, et al., J. Hazard. Mater. 403 (2021) 123979.
[13] J. Zheng, D. Song, H. Chen, et al., Chin. Chem. Lett. 31 (2020) 1109–1113.
[14] L. Guo, S. Chen, Y.L. Yu, et al., Anal. Chem. 93 (2021) 16240–16247.
[15] X. Han, L. Liu, H. Gong, et al., Food Chem. 371 (2022) 131115.
[16] H. Rao, X. Xue, M. Luo, et al., Chin. Chem. Lett. 32 (2021) 25–32.
[17] P.T. Nguyen, J. Lee, A. Cho, et al., Adv. Funct. Mater. 32 (2022) 2112428.
[18] R.W. Tarnuzzer, J. Colon, S. Patil, et al., Nano Lett. 5 (2005) 2573–2577.
[19] E. Shoko, M.F. Smith, R.H. McKenzie, J. Phys. Condens. Matter 22 (2010) 223201.
[20] N. Shehata, K. Meehan, M. Hudait, et al., J. Nanopart. Res. 14 (2012) 1173.
[21] Z. Wang, R. Zhang, X. Yan, et al., Met. Prog. 41 (2020) 81–119.
[22] H. Cheng, S. Lin, F. Muhammad, et al., ACS Sens. 1 (2016) 1336–1343.
[23] J. Xi, G. Wei, L. An, et al., Nano Lett. 19 (2019) 7645–7654.
[24] W.Y. Hernández, O.H. Laguna, M.A. Centeno, et al., J. Solid State Chem. 184 (2011) 3014–3020.
[25] F. Muhammad, A. Wang, W. Qi, et al., ACS Appl. Mater. Interfaces 6 (2014) 19424–19433.
[26] Z.H. Yang, S. Ren, Y. Zhuo, et al., Anal. Chem. 89 (2017) 13349–13356.
[27] M. Yang, G. Shen, Q. Wang, et al., Molecules 26 (2021) 6363.
[28] I.V. Zagaynov, I.V. Shelepin, S.V. Fedorov, et al., Ceram. Int. 47 (2021) 22201–22208.
[29] M. Godinho, M.H.M. Rodrigues, R.D.F. Gonçalves, et al., Mater. Sci. Eng. B 266 (2021) 115060.
[30] Y. Li, Y. Li, H. Wang, R. Liu, ACS Appl. Mater. Interfaces 13 (2021) 13968–13977.
[31] W. Guo, M. Zhang, Z. Lou, et al., ChemCatChem 11 (2019) 737–743.
[32] M. Zhu, Y. Wen, S. Song, et al., Nanoscale 12 (2020) 19104–19111.
[33] M. Wang, H. Zhu, B. Liu, et al., ACS Appl. Mater. Interfaces 14 (2022) 44762–44771.
[34] Y. Chen, C. Zhao, G. Yue, et al., Food Chem. 317 (2020) 126361.
[35] W. Li, Y. Shi, X. Hu, et al., Food Control 106 (2019) 106704.
[36] H. Wang, L. Da, L. Yang, et al., J. Hazard. Mater. 392 (2020) 122506.